Journal of Marine Research, 49, 467–492, 1991

Time scales of mesoscale variability and their relationship with space scales in the North Atlantic

by P.Y. Le Traon[1]

ABSTRACT

A systematic study of characteristic time scales of mesoscale variability over the North Atlantic was done using two years of Geosat data. Time scales are first characterized by 10° latitude by 10° longitude bins. A more detailed description was obtained by globally mapping the Sea Level Anomaly temporal correlation after one cycle (17.05 days). The scales are shortest in areas of high mesoscale activity (Gulf Stream, North Atlantic Current) while relatively long time scales are observed over the Mid-Atlantic Ridge and in the eastern part of the basin. In general, time scales are not proportional to space scales. Propagation velocities obtained by dividing space scales by time scales appear to be minimal east of the Mid-Atlantic Ridge. Frequency-wavenumber spectral analysis complemented this statistical description of mesoscale variability. It shows that the dominant wavelengths of around 200 to 500 km (depending on latitude) are associated with long periods (> 150 days) in the eastern part of the basin, while near the Gulf Stream significant energy is found at shorter periods. Propagation velocities are generally westward. Pseudo-dispersion relations deduced from Geosat data suggest two distinct dynamic regimes, as in quasigeostrophic turbulence models: a turbulent regime for smaller scales, with proportionality between space and time scales, and an apparently more linear regime where an inverse dispersion relation is found in the eastern part of the basin. This latter characteristic is in agreement with quasigeostrophic models forced by fluctuating winds.

1. Introduction

The US Navy's Geosat altimeter (1985–1989) has provided new capabilities for mesoscale observations (Cheney *et al.,* 1986). The satellite operated on a near-repeat orbit (17.05-day cycle) for almost three years (November 86–June 89), with temporal (and spatial) sampling well suited to mesoscale studies (e.g. Fu and Zlotnicki, 1989; Le Traon *et al.,* 1990). Extensive, global spatio-temporal sampling is a unique means of providing a statistical description of mesoscale phenomena. Such a description can reveal differences between ocean regions and help to understand eddy dynamics, particularly the mechanisms which generate and dissipate eddies (e.g. Zlotnicki *et al.,* 1989). This data analysis also seems necessary before using the data in models

1. CLS Argos, 18 Avenue Edouard Belin, 31055 Toulouse cedex, France.

(e.g. De Mey and Menard, 1989) and can be usefully compared with the results generated by modeling (e.g. White *et al.,* 1990).

A global statistical description of mesoscale variability in the North Atlantic with Geosat data has been started by Le Traon *et al.* (1990). They have conducted a systematic study of wavenumber spectra and have characterized the space scales of mesoscale variability. Their results provide a good match with *in-situ* data and compare qualitatively with quasigeostrophic turbulence models. Wavenumber spectra are thus consistent with eddy forcing by instability of a mean current in the western side of the basin and with wind forcing on the eastern side. This paper extends the analysis to mesoscale variability time scales and their relationship with space scales over the North Atlantic.

The paper is organized as follows: Section 2 describes the calculation of temporal autocorrelation functions and the characterization of time scales. These are compared with space scales. The relationships between time and space scales are then detailed in Section 3 through frequency-wavenumber spectral analysis. Section 4 summarizes the principal results and provides the main conclusions.

2. Time scales

a. Altimeter data processing and calculation of time scales

Since one of the objectives of this study was to compare time scales with space scales, the data set and altimetric data processing methods are those used by Le Traon *et al.* (1990) who calculated the space scales. The data set comprises two years of Geosat Geophysical Data Records (GDRs) spanning the period from November 1986 to November 1988, i.e. 44 cycles of 17.05 days. The procedures applied to process these data are described in detail in Le Traon *et al.* (1990) and will only be briefly recalled here:

The sea surface height measurements (SSH) were first corrected for the following effects (corrections available in the GDRs): electromagnetic bias by adding 2% of significant waveheight ($H_{1/3}$) to the SSH, ocean tides using the Schwiderski model, terrestrial tides with the model of Cartwright and Taylor, ionospheric effects using the Global Positioning System climatic model, and dry and wet tropospheric effects using Fleet Numerical Oceanography Center data (Cheney *et al.,* 1987). Because of the uncertainties of estimating an inverted barometer correction (see Zlotnicki *et al.,* 1989), none was applied.

The study area (20N–60N, 70W–10W) was then divided into four 10°-latitude strips between 20N and 60N, corresponding to 1500-km arc segments (Fig. 1). SSH profiles were resampled every 10 km using a cubic spline to provide regular sampling (the initial sampling rate is 6.8 km). The mean profile was then subtracted from each individual profile. A first-degree polynomial adjustment was performed to eliminate long-wavelength components, basically orbit related. This gives the mesoscale Sea Level Anomaly (SLA), sampled every 10 km, at the time of the satellite pass on the

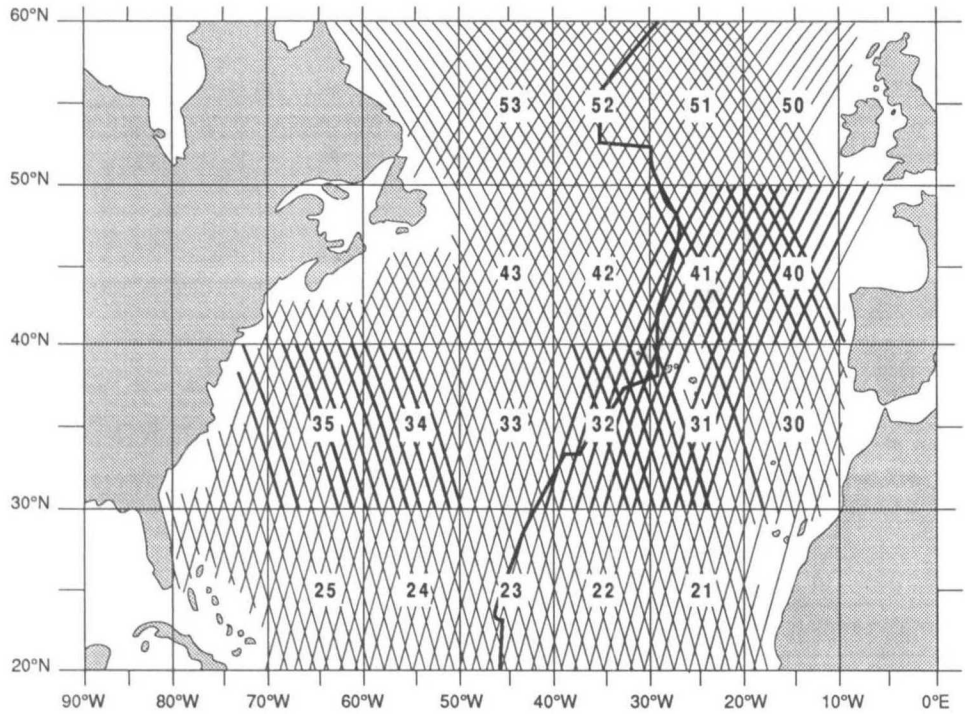

Figure 1. The study area, in the North Atlantic between 20N and 60N, where Geosat tracks used are overlaid. The two-figure numbers correspond to groups of 10° (latitude) × 10° (longitude) bins where wavenumber spectra and temporal and spatial autocorrelation functions have been systematically calculated. Mid-Atlantic Ridge is also shown. Bold lines correspond to tracks used for frequency-wavenumber spectrum calculations (see Section 3).

given track. The SLA data were then smoothed by a Lanczos filter (Hamming, 1977) with a cutoff wavelength of 100 km.

The time scales for different parts of the North Atlantic basin were first characterized by groups of 10° latitude by 10° longitude as in Le Traon *et al.* (1990). Each group was assigned a two-figure number, the first giving the strip number (2 through 5 for latitudes from 20N through 50N) and the second the longitude (0 through 5 for 10W through 60W) (Fig. 1). There were an average of about 13 tracks per group.

For each track belonging to a given group, the temporal covariance $C(\tau)$ was estimated at each point (every 10 km) as follows:

$$C_{\text{est}}(\tau) = \sum_{i=1}^{NT-j} \text{SLA}(t_i)\text{SLA}(t_i + \tau)/NT \qquad \text{with } t_i = (i-1) \times 17 \text{ and } \tau = j \times 17 \quad (1)$$

(NT is number of cycles, 44 if data set is complete; j is the cycle number).

An average is then calculated for the set of points on each track in the group and data were normalized by the SLA variance. The mean autocorrelation function was

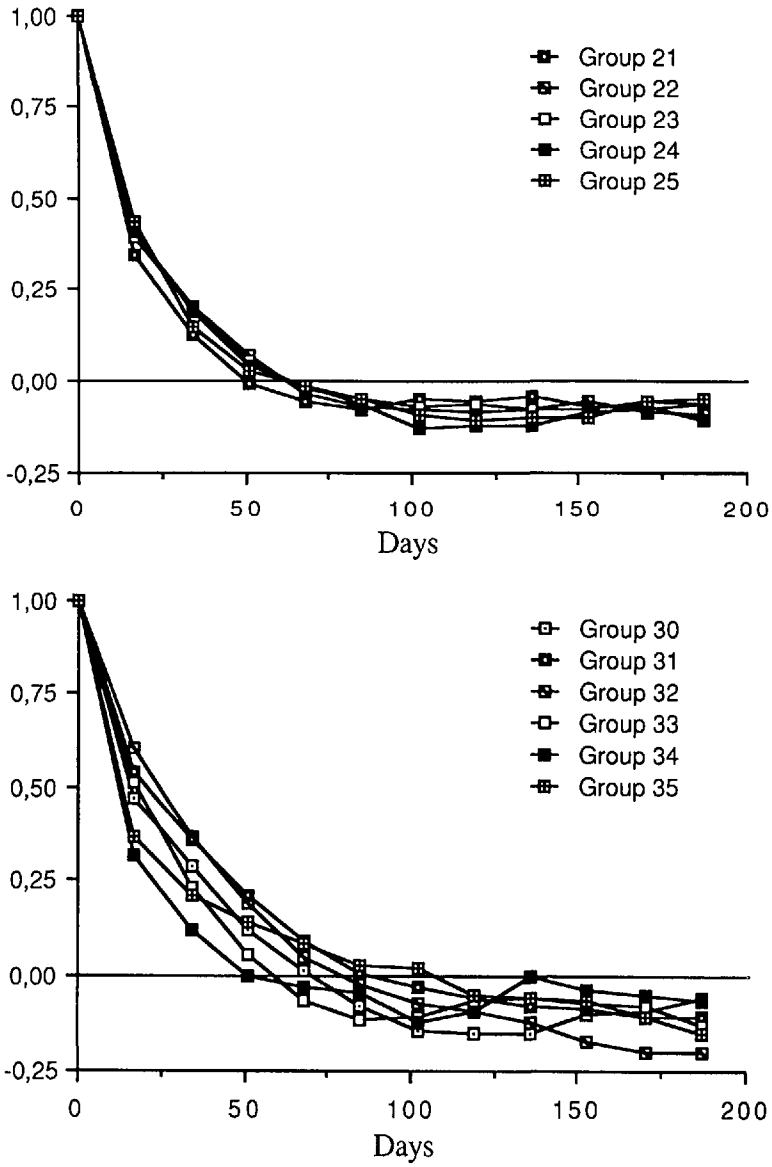

Figure 2. (a) Mean temporal autocorrelation function for groups between 20N and 30N. (b) Mean temporal autocorrelation function for groups between 30N and 40N. (c) Mean temporal autocorrelation function for groups between 40N and 50N. (d) Mean temporal autocorrelation function for groups between 50N and 60N.

then obtained by averaging the different tracks in the group. Note that the temporal autocorrelation functions at each point were not necessarily calculated from complete time series, since certain cycles are gappy or missing. The functions thus obtained are shown in Figures 2 a, b, c and d.

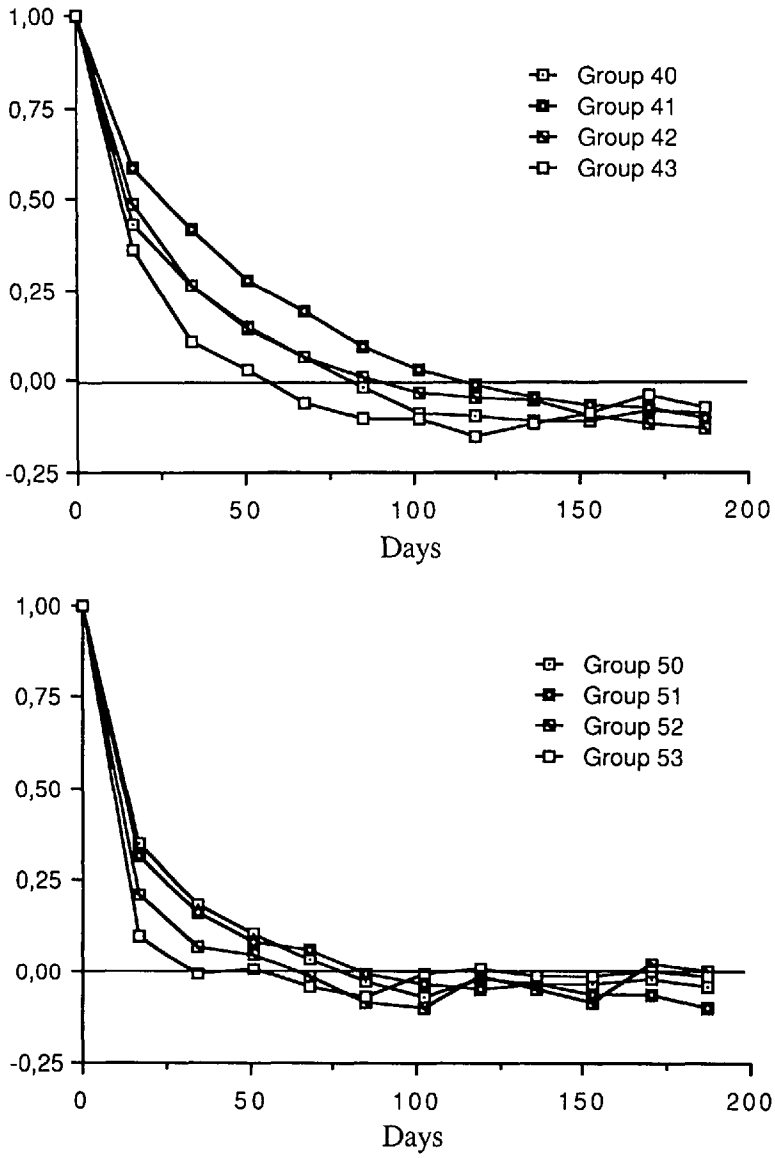

Figure 2. (Continued)

To examine the time scales and their variations in greater detail, we calculated the 17-day isocorrelations $C_{est}(17)/C_{est}(0)$ in 2° latitude by 2° longitude bins. Objective analysis (Bretherton *et al.*, 1976) was applied to map this value while smoothing out small-scale variations. Spatial autocorrelation functions of the mapping were chosen as Gaussian with standard deviations of 2° in latitude and 3° in longitude. The errors on the estimation of the 17-day covariances in each bin (which are needed for

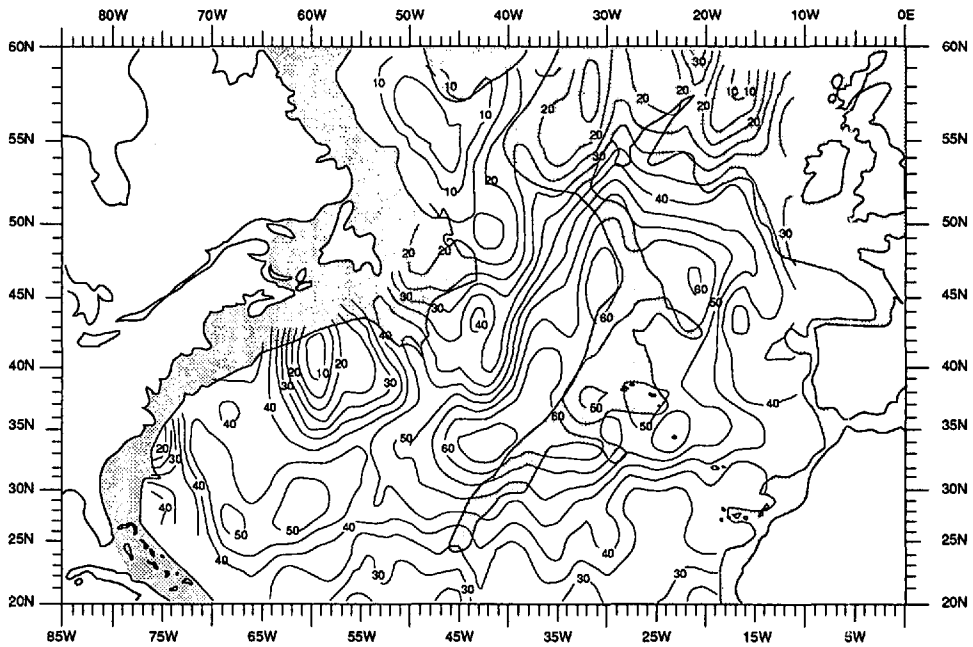

Figure 3. 17-day isocorrelation map (×100) of altimetric Sea Level Anomalies. Depths shallower than 3000 m are shaded.

objective analysis) were calculated as described in the next section, i.e. assuming spatial decorrelation of 100 km, and also assuming quasi-normality. Figure 3 shows the 17-day isocorrelation map in percent obtained after objective analysis and contouring.

b. Statistical accuracy and major sources of error

To calculate the error on estimation of the temporal covariances, we assumed spatial decorrelation of 100 km along the profiles (≈first zero crossing of spatial autocorrelation function). We thus had roughly 15 independent temporal series per track (the tracks are 1500 km long). If we assume the tracks to be independent (inter-track distance > 100 km), there are at least 150 independent temporal series, of maximum length two years, per group (there are at least 10 tracks per group). For each temporal series, $e^2(\tau)$ [$e^2(\tau) = \langle [C_{est}(\tau) - C(\tau)]^2 \rangle$ (where $\langle . \rangle$ stands for mathematical expectation)], the theoretical error on the estimation of covariances $C(\tau)$ can be calculated assuming quasi-normality. $e^2(\tau)$ is expressed simply from the fourth-order moments and this assumption provides a means of relating the fourth-order moments $\langle \mathrm{SLA}(t_i)\mathrm{SLA}(t_j)\mathrm{SLA}(t_k)\mathrm{SLA}(t_l) \rangle$ to the second-order moments, i.e. to the covariances (e.g. Monin and Yaglom, 1971). We calculated the typical error $e^2(\tau)$ for the altimetric covariances, and divided the error by the mean number of degrees of freedom, i.e. 150 according to our estimates. We took a pessimistic viewpoint,

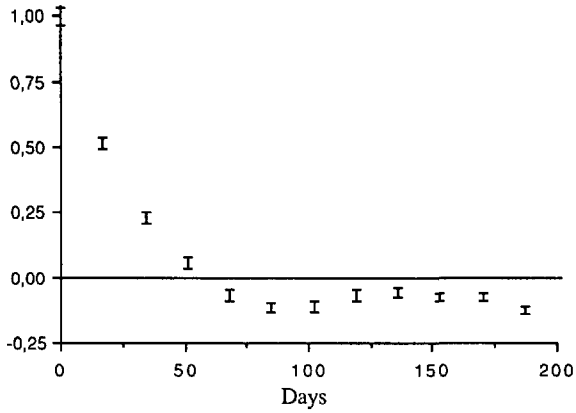

Figure 4. Confidence intervals, one standard deviation, on estimation of temporal autocovariance functions.

assuming the temporal series to be one year long ($NT = 22$), as most of the series are incomplete. The one standard deviation confidence intervals $[\pm e(\tau)/\sqrt{150}]$ are shown in Figure 4. The figure shows that the statistical accuracy on the above functions (Fig. 2a, 2b, 2c and 2d) is very good, and in particular that most of the differences between groups are statistically significant. Similarly, the error map corresponding to Figure 3 (17-day isocorrelation map), which is not shown here, gives a uniform rms error of below 10%, which shows that the observed variations are statistically significant. This is confirmed by the shape of the 17-day isocorrelation map which is not very noisy even without smoothing by objective analysis. Note that, strictly speaking, the errors on correlations $C(\tau)/C(0)$ should be slightly different from those on covariances $C(\tau)$, calculated here because of errors on the estimation of the variance $C(0)$.

The above accuracies are only statistical and do not account for altimetric measurements errors. For our mesoscale study, these are essentially sea state bias, tropospheric and inverse barometer effects. All these atmospheric effects are associated with shorter time scales than the oceanic time scales and the more significant ones could cause underestimation of time scales. However, it seems that these errors are globally well below the oceanic signal. Indeed, Jourdan (1990) has shown that for mesoscale studies, these three errors have a combined variance of typically 10% that of the mesoscale signal in the Northeast Atlantic. Other studies confirm that Geosat data are not over-contaminated by these effects in mid-latitude regions (e.g. Bisagni *et al.,* 1989; Monaldo, 1990; Zlotnicki *et al.,* 1989). This means that except for very low energy regions, time scales are probably only slightly affected by atmospheric effects. Note, however, that recent analyses with SSM/I (Special Sensor Microwave Imager) data show that errors due to tropospheric fronts can significantly affect our SLA estimations for about 20% of the time (Jourdan, personal communication).

Another source of error must be considered in temporal studies. This is the error due to polynomial adjustment of altimetric profiles to reduce the long wavelength orbit error. Le Traon *et al.* (1991) have shown that the variance of this error is typically 10% of the variance of the oceanic signal for the adjustment used in this study (first degree over 1500 km). However, since this error is due to removing part of the oceanic signal by the polynomial adjustment, it will not generally affect the temporal correlation of the residual oceanic signal significantly. This is certainly not true, however, when the ocean signal is strongly nonhomogeneous. In such cases, the error can then be greater than the ocean signal (Le Traon *et al.,* 1991). Inspection of Figure 3 shows, however, that the effects of polynomial adjustment on temporal correlation in the strongly nonhomogeneous area of the Gulf Stream are not very significant. Indeed, there is good agreement between the temporal correlations calculated between 30N and 40N and between 20N and 30N. At the worst, the temporal correlations between 30N and 35N in the western part of the basin may be slightly underestimated because of the leakage from the highly energetic and weakly temporally correlated area of the Gulf Stream.

c. Discussion

The temporal auto-correlation functions (Fig. 2a, b, c, d) show clear differences between the various groups. The first zero crossings range from 34 days (group 53) to 119 days (group 41). There are significant differences according to longitude, except for strip 2 (20N–30N). There is a trend of time scales diminishing westward. The longest time scales are observed in the eastern part (e.g. groups 41, 31 and 32).

The integral time scales $L1$, defined in (2) below, summarize the evolution of time scales according to latitude and longitude (Fig. 5).

$$L1 = \int_0^{zc} C(t)/C(0)\, dt, \qquad (zc = \text{first zero crossing of } C) \tag{2}$$

The 17-day isocorrelation map (Fig. 3) illustrates these variations in a more detailed manner. The westward decrease with longitude is clear. In general, areas of weak temporal correlation are associated with areas of high mesoscale activity, as can be seen by comparing Figure 4 with the SLA variability map calculated by Le Traon *et al.* (1990). These areas of weak temporal correlation thus also correspond to areas of strong mean currents (i.e. the Gulf Stream and the North Atlantic Current), which are important source of eddy energy through instability.

On the other hand, in the eastern part of the basin where mean currents are weaker, the two areas where the strongest temporal correlation is observed are the two current branches which cross the Mid-Atlantic Ridge (e.g. Saunders, 1982). These lie north and south of the Azores Islands, i.e. around 35N and north of 45N. Thus, the Azores current which crosses the ridge between 32N and 36N (Gould, 1985; Klein and Siedler, 1989) is associated with strong temporal correlations

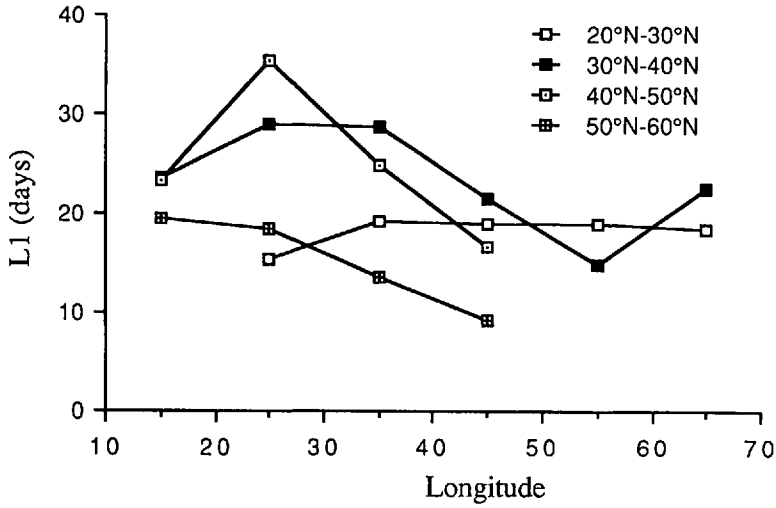

Figure 5. Evolution of $L1 = \int_0^{zc} C(z)/C(0)\, dz$ (C = SLA temporal autocovariance function; zc = first zero crossing of C) according to longitude for strips 2, 3, 4, 5.

(17-day isocorrelations greater than 0.5). The long time scales observed in the region and more generally in the Northeast Atlantic can be related, in part, to a low frequency signal and particularly to a seasonal signal which is relatively stronger than in the Gulf Stream area. Indeed, the analyses by Stramma and Siedler (1988) and Klein and Siedler (1989) reveal significant seasonal variations in the Azores current and the eastern part of the subtropical gyre.

Finally, comparing 17-day isocorrelation map with the bathymetry of the North Atlantic (Fig. 3) also suggests that the bottom topography plays an important role in the temporal coherence of mesoscale structures. It can thus be seen that the areas with the highest temporal correlation (17-day isocorrelation > 0.5) coincide with the Mid-Atlantic Ridge. Temporal correlation then diminishes more rapidly west of the ridge than east in the Gulf Stream and North Atlantic areas.

i. Comparison with currentmeter data measurements. The increase of time scales with longitude was already suspected by Richman *et al.* (1977) and Wunsch (1983). They used the MODE and POLYMODE data to show that time scales tend to lengthen eastward along 28N. Although larger variations in time scales are found farther north, this agrees with Geosat data. Apart from strip 2 (20N–30N), the scales tend to diminish northward. In his statistical analysis of long term current meter moorings, Dickson (1983) noted that the dominant time-scale of low frequency motions appears to decrease progressively northward in the western basin. The transect he studied comprises essentially POLYMODE current meter data. Its southern tip is near 30N–60W in the deep interior of the gyre. The time scales are the longest here, in agreement with Figure 3 where a local maximum of temporal correlation (17-day

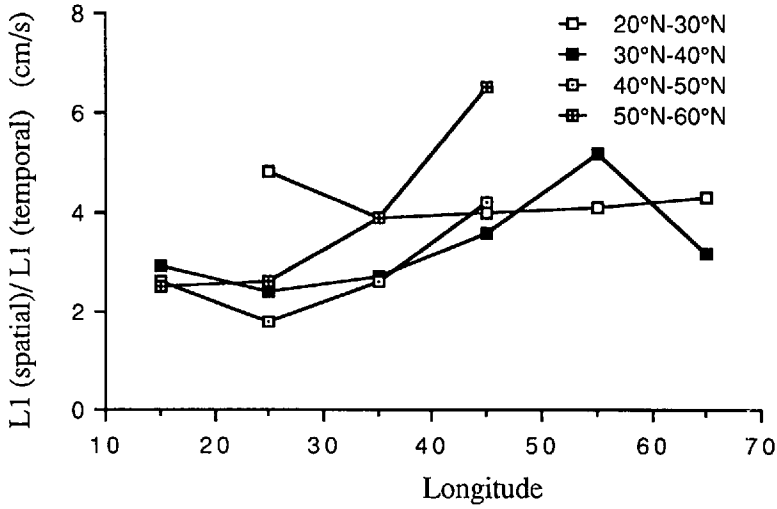

Figure 6. Evolution of C (C = integral space scales/integral time scales) according to longitude for strips 2, 3, 4, 5 (in cms^{-1}).

isocorrelation >0.5) is found near 30N–60W. Time scales decrease farther north, near 55W, as is also clearly seen on Figure 3. Lippert and Briscoe (1990) using the LOTUS data (34N–70W) have shown that this northward decrease of time scales is not clear along 70W, a result consistent with the N/S orientation of 17-day SLA isocorrelation contours at 70W. Current meter measurements have also been obtained along 48N, during the French-German TOPOGULF experiment. Four clusters of current meter moorings were deployed on each side of the Mid-Atlantic Ridge from 35W to 20W. Colin de Verdiere *et al.* (1989) have shown that the 35W cluster had the shortest time scales at the surface, the other three having similar time scales. This can also be observed qualitatively on Figure 3. The long time scales seen in the North-East Atlantic are also to be compared with the rather low-frequency motions found at some of the North-East Atlantic Dynamic Studies (NEADS) sites (Gould, 1982).

ii. Comparison between integral time and space scales. Figure 6 shows the evolution of C, which is the division of integral space scales $L1$ [as calculated by Le Traon *et al.* (1990)] by integral time scales $L1$ (as calculated above), as a function of latitude and longitude. C translates as a propagation velocity (in cms^{-1}) and is the typical velocity at which structures pass a fixed point. It varies on a scale of one to four, and in general the space and time scales are not proportional. The space scales increase mainly with longitude (Le Traon *et al.*, 1990), while time scales decrease with longitude. As a consequence, these velocities increase significantly westward (except between 20N and 30N). This suggests that the larger structures observed in the west move more quickly. On the other hand, east of the ridge (apart from strip 2), the

velocities are roughly uniform, around 2 cms^{-1}, indicating a proportional relationship between the space and time scales. It is also east of the ridge that the lowest propagation velocities, related to the long time scales, are observed.

A more detailed description of the relationship between time and space scales can be obtained through frequency-wavenumber spectral analysis. This will be done in the next section.

3. Frequency-wavenumber spectral analysis

a. Methods

The frequency-wavenumber spectra can be calculated fairly simply by two-dimensional Fourier transform (see, for example, Parke, 1990; White *et al.,* 1990), but requires complete (time- and space-continuous) series. This is not really true of Geosat data, which has missing or gappy cycles. The first stage in calculating the spectrum is thus to select good tracks and/or fill in gaps. The procedure is as follows, track by track:

(1) for each cycle, the gaps are filled by linear interpolation. If there are more than three consecutive gaps (40 km) or more than 10% missing points, the profile is rejected. If the length of the track with common validated points is shorter than 1000 km, the track is rejected.

(2) linear interpolation is then done between the different cycles to overcome gaps and rejects. If there are more than two consecutive gappy cycles, no interpolation is done. The longest possible temporal series common to all points on the track is then selected. If the temporal series is shorter than one year, the track is rejected.

(3) complete spatio-temporal series of at least 1000 km and one year are obtained for selected tracks. These series are filled out with zeroes to obtain series of 1500 km and two years. This provides spectral estimates common to all the tracks.

From a space-time series SLA(x, t) on a track of length L (L = 1500 km) and duration T (T = 2 years), the 2D spectrum is calculated by 2D FFT. This means calculating the Fourier A_{nm} coefficients such that:

$$\mathrm{SLA}(x,t) = \sum_{n,m=-\infty}^{\infty} A_{nm} e^{j(knx+\omega mt)} \qquad \text{where } k = 1/L \text{ and } \omega = 1/T. \tag{3}$$

Considering only the purely periodic part of the signal ($n \neq 0$ and $m \neq 0$), SLA(x, t) can be expressed as follows:

$$\mathrm{SLA}(x,t) = \sum_{n,m=1}^{\infty} A_{nm} e^{j(knx+\omega mt)} + A_{-n-m} e^{-j(knx+\omega mt)} + A_{n-m} e^{j(knx-\omega mt)} + A_{-nm} e^{j(-knx+\omega mt)}. \tag{4}$$

The first two terms (A_{nm}, A_{-n-m}) correspond to waves which propagate as x decreases (retrogressive waves), while the last two (A_{n-m}, A_{-nm}) correspond to waves propagat-

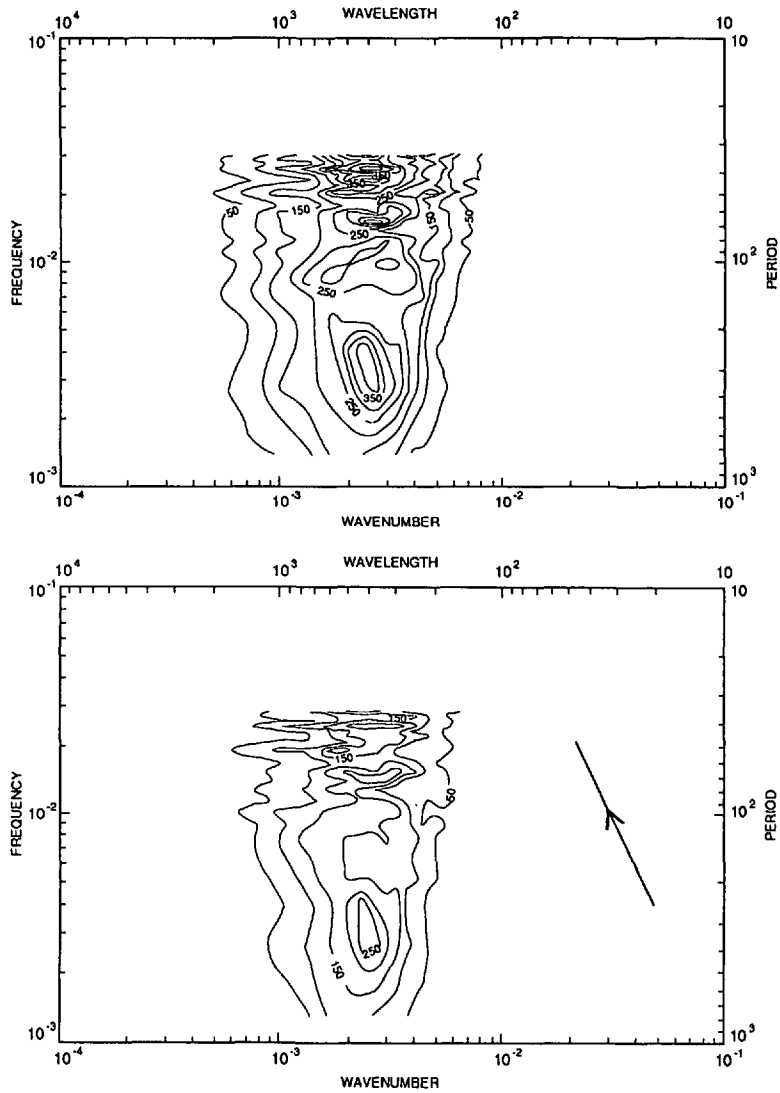

Figure 7. (a) Total frequency-wavenumber spectrum for the Gulf Stream area (30N–40N; 70W–50W). Units are cm^2. Contour interval is 50 cm^2. (b) Frequency-wavenumber spectrum for the Gulf Stream—northwest propagation. (c) Frequency-wavenumber spectrum for the Gulf Stream—southeast propagation.

ing as x increases (progressive waves). The spectral energy S_{nm} is defined as follows:

$$S_{nm} = |A_{nm}|^2 + |A_{-n-m}|^2 + |A_{n-m}|^2 + |A_{-nm}|^2.$$

The x coordinate represents positions on the track oriented in the sense of increasing latitude. A_{nm} and A_{-n-m} thus represent the amplitudes of waves propagating south-eastward (ascending tracks) or south-westward (descending tracks). A_{n-m} and A_{-nm}

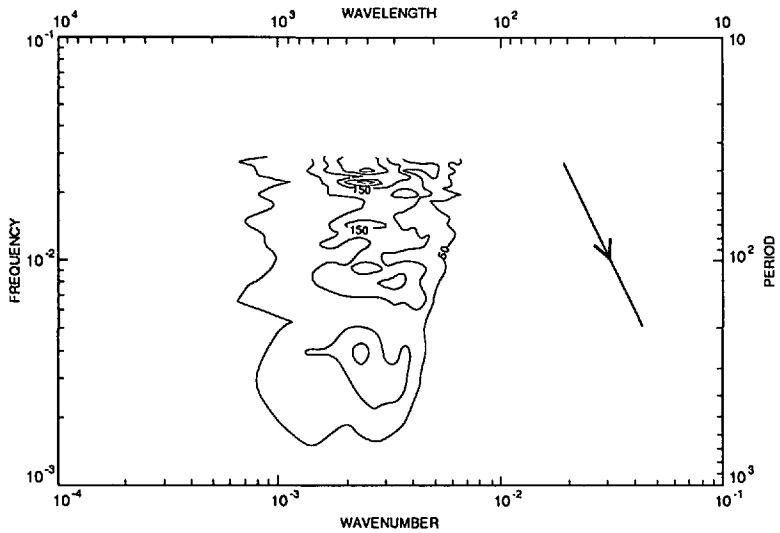

Figure 7. (Continued)

represent the amplitudes of waves propagating north-westward (ascending tracks) or north-eastward (descending tracks). For a given wave, we in fact obtain the projection of the wave vector onto two directions (ascending and descending tracks). By combining the information, we can estimate the directions (and velocities) with which the structures propagate for a given wavenumber. Thus, a wave propagating westward will only be "seen" on spectra of northwest ascending tracks and southwest descending tracks. Note that the wavelengths (and propagation velocities) "seen" on the tracks will be overestimated by a factor of $1/\cos\theta$ (where θ is the angle between the track and the wave vector). In practice, however, it is difficult to distinguish between a wave propagating westward and two waves propagating northwest and southwest. This limitation is related to spatial aliasing, inherent in all one-dimensional (in space) spectral calculations. Note also that the equipartition of energy between progressive and retrogressive waves can be interpreted as quasi-standing wave oscillations (Hayashi, 1973).

We chose three typical zones of around 10° in latitude by 20° longitude (see Fig. 1), for which we calculated the mean frequency-wavenumber spectra: the Gulf Stream (30N–40N, 70W–50W), Azores Current (30N–40N, 40W–20W), and Northeast Atlantic (40N–50N, 30W–10W). We have 12, 19 and 19 selected tracks for the GS, AC and NEA zones respectively.

Assuming that one track in three is independent ($\approx$300 km), this yields about 20 degrees of freedom for the spectral estimations, i.e. a 90% confidence interval of $\pm$40%. These are only crude estimates of the number of degrees of freedom, since neighboring tracks are differently correlated for different frequencies and wavenumbers. However by choosing a decorrelation of one track in three, which is around

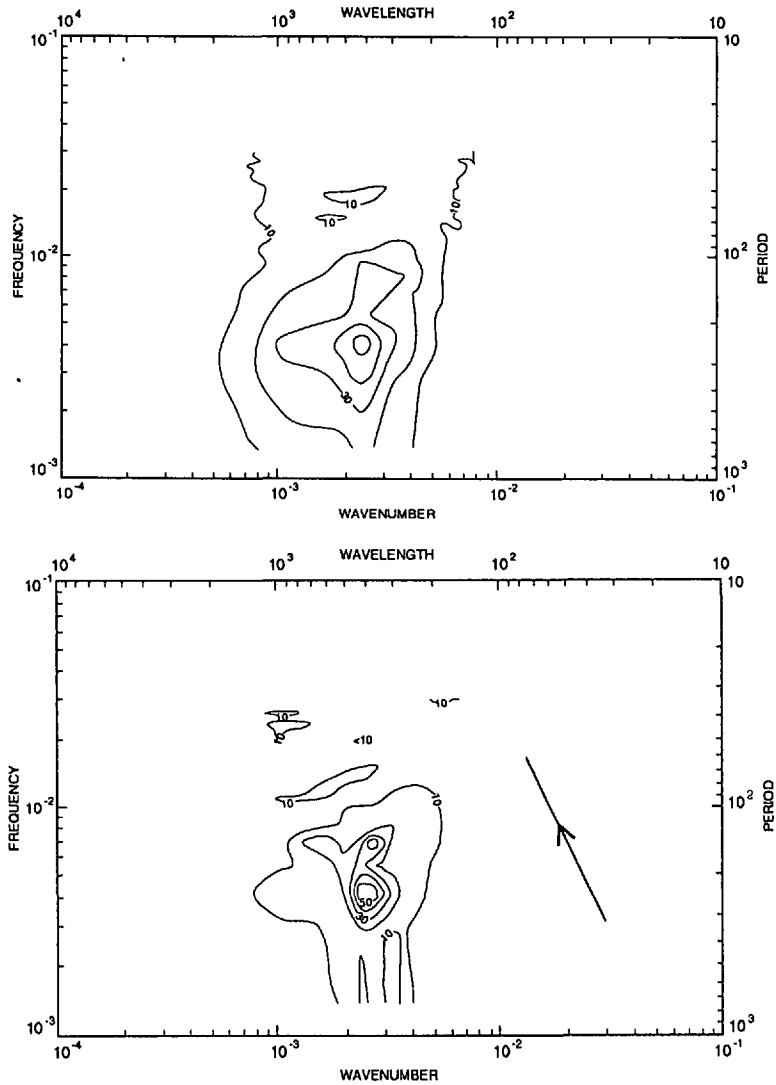

Figure 8. (a) Total frequency-wavenumber spectrum for the Azores Current area (30N–40N; 40W–20W). Units are cm^2. Contour interval is 10 cm^2. (b) Frequency-wavenumber spectrum for the Azores Current—northwest propagation. (c) Frequency-wavenumber spectrum for the Azores Current—southeast propagation. (d) Frequency-wavenumber spectrum for the Azores Current—northeast propagation. (e) Frequency-wavenumber spectrum for the Azores Current—southwest propagation.

three times the actual spatial decorrelation length of SLA measurements (Le Traon *et al.,* 1990), our error estimates are probably conservative. The assumption of stationarity and homogeneity implicit in the calculation is also probably not realistic, but the size of the areas is dictated by the periods and wavelengths of interest (up to 1500 km and 2 years) and the need for a sufficient number of tracks. The spectra may

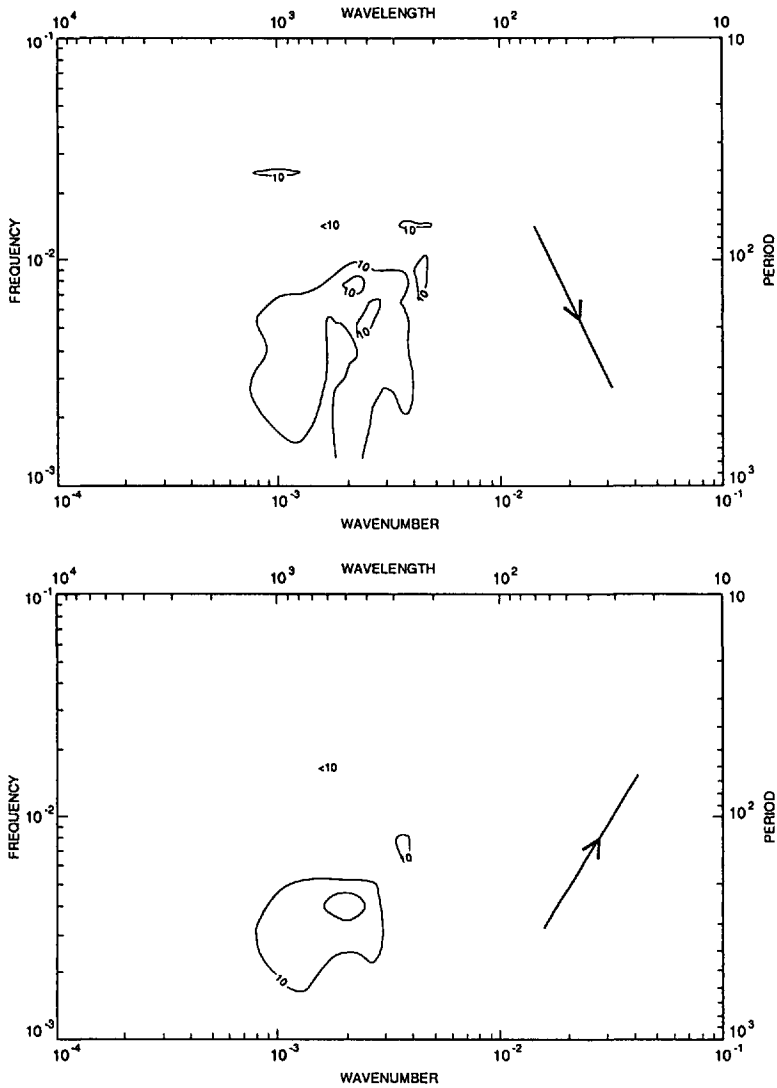

Figure 8. (Continued)

thus be more representative of certain more energetic subregions (in space and/or in time), or else signals characteristic of different sub-regions may be observed in the same spectrum. The GS area contains ascending tracks only, and we calculated the total mean spectrum (Fig. 7a), the north-westward propagation spectrum (Fig. 7b), and the south-eastward propagation spectrum (Fig. 7c). For the other two areas, we calculated the total spectrum (Fig. 8a [AC] and Fig. 9a [NEA]) and the spectra for all directions along ascending and descending tracks (Fig. 8b to Fig. 8e [AC] and Fig. 9b to Fig. 9e [NEA]). Note that these spectra are shown in a variance-preserving form,

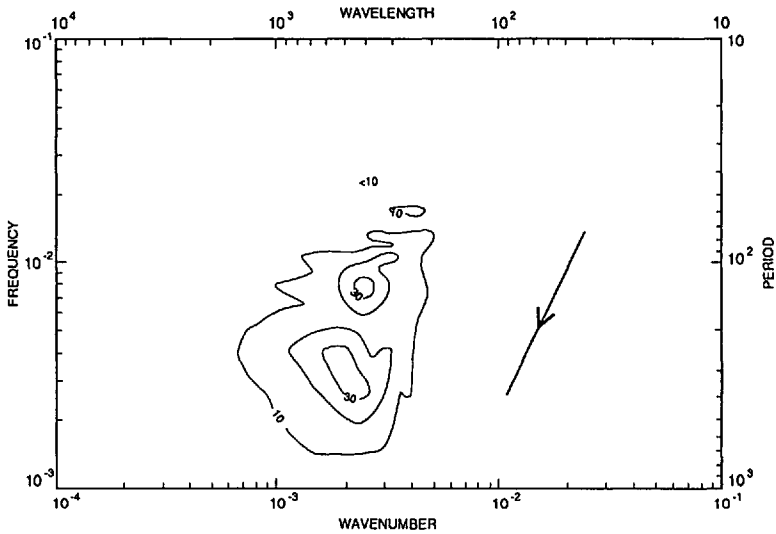

Figure 8. (Continued)

i.e. that the spectral energies have been multiplied by the wavenumbers and frequencies. On a logarithmic scale, this provides spectral energy proportional to volume.

b. Results and discussion

The mean spectrum for the GS region (Fig. 7a) shows that the energy corresponds mainly to wavelengths between 200 and 600 km over a broad range of periods, from the shortest observable (34 days) to over 400 days. There is probably aliasing of the shorter periods onto longer periods. The Nyquist frequency of 34 days^{-1}, which is the upper limit for frequencies observable by Geosat, certainly places a limit on the observation of certain mesoscale structures in the Gulf Stream. Significant energy is observed over short periods (<80 days) at wavelengths of 300 to 500 km. These mesoscale structures propagate both north-westward and south-eastward, with a balanced distribution of spectral energy between the two directions (see Fig. 7b and Fig. 7c). The corresponding propagation velocities are on the order of 10 cms^{-1}. If we assume that they are mainly zonal, then they are either westward or eastward (in this case, they would also be over-estimated by a factor of roughly 2 because of the angle between the tracks and the zonal direction). These structures could be the signatures of Gulf Stream rings and meanders, which have periods and wavelengths of a few months and a few hundred kilometers respectively (Richardson, 1983). The Gulf Stream rings have, in addition, propagation velocities on the order of 5 cms^{-1} which are either eastward (advection by mean current) if they are in the Gulf Stream or westward (propagation like a Rossby wave packet) if they are not. We observe another spectral peak for a wavelength of around 400 km but at lower frequencies

close to one year. It would be useful to relate this seasonal signal to variations in the transport and/or mean position of the Gulf Stream. The Gulf Stream does, indeed, have an annual cycle (Stommel, 1965) and Fu *et al.* (1987) observed it with GEOS-3 altimetric data. The signal observed by Geosat propagates mainly westward (propagation velocity on the order of 1 cms^{-1}) as it is mainly seen on Figure 7b (north-westward propagation). Note, however, that given the maximum length of our time series (2 years), the spectral peaks seen at the one-year frequency are also to be related to an underestimation of the 2-year frequency spectrum.

The mean spectra of the other two zones in the eastern part of the basin (Fig. 8a, AC and Fig. 9a, NEA) are different from the above spectrum. Short periods are characterized by low energy, particularly in the AC area, where the signal is very weak for periods shorter than 80 days. The AC area has an energy peak between 300 and 400 km and 100 and 200 days. This signal is seen mainly on the westward propagating spectrum of ascending tracks and descending tracks (Fig. 8b and Fig. 8e). If one agrees with this westward propagation, the true signal has typically a wavelength of 150–200 km and a period of 150 days. It probably corresponds to eddies associated with meandering of the Azores current, which is the main source of eddy energy in this particular area (Gould, 1985; Käse *et al.,* 1985; Siedler *et al.,* 1985). There is also a lower frequency quasi-seasonal signal for wavelengths between 300 and 600 km, which also propagates westward as it can be seen on the spectra of north-west ascending tracks and south-west descending tracks. The NEA area farther north has smaller space scales (see also Le Traon *et al.,* 1990). Significant energy is noted for wavelengths between 200 and 300 km and periods of 150 to 400 days. This signal apparently propagates south-westward (Fig. 9e), i.e. parallel to the ridge. There is another spectral peak, corresponding to a seasonal signal, with wavelengths in the 300 to 600 km range, which propagates westward (Fig. 9b and Fig. 9e). The signal in the NEA area is apparently dominated by these low-frequency and quasi-seasonal motions, which agrees with the corresponding NEADS measurements (Gould, 1983). Eddies observed during the Tourbillon experiment (47N, 13.5W) (Le Groupe Tourbillon, 1983) were found in the 64–150 day period band and in the 100–200 km wavelength band (Mercier and Colin de Verdière, 1985). Although they are present in the above spectra, they do not seem to be representative of the mean spectral characteristics of the rather large area studied here.

Observation of the seasonal signal from Geosat altimeter data is difficult because of the approximate atmospheric corrections. Zlotnicki *et al.* (1989) have nevertheless observed that the Northeast Atlantic is one of the ocean areas where Geosat altimeter data shows the strongest seasonal variation. After analyzing their effects, they also concluded that geophysical corrections could not explain the seasonal signal observed. The presence of a noticeable seasonal signal in the Northeast Atlantic is confirmed by our spectral analysis, which also provides partial validation of the results, since the characteristics of the observed signal (wavelengths and

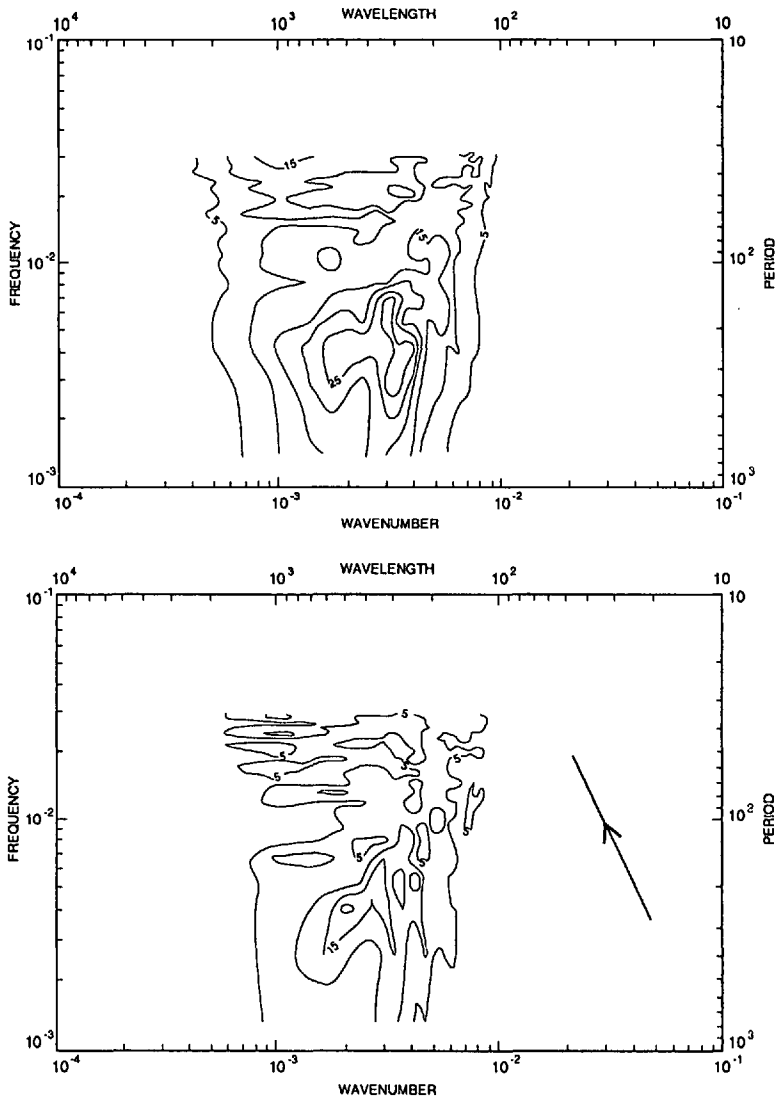

Figure 9. (a) Total frequency-wavenumber spectrum for the Northeast Atlantic area (40N–50N; 30W–10W). Units are cm^2. Contour interval is 5 cm^2. (b) Frequency-wavenumber spectrum for the Northeast Atlantic—northwest propagation. (c) Frequency-wavenumber spectrum for the Northeast Atlantic—southeast propagation. (d) Frequency-wavenumber spectrum for the Northeast Atlantic—northeast propagation. (e) Frequency-wavenumber spectrum for the Northeast Atlantic—southwest propagation.

mainly westward propagations) are more typical of an ocean signal than of an atmospheric signal (Willebrand, 1978). More generally, however, frequency-wavenumber spectral analysis of the major sources of error would be necessary for a better validation of these results.

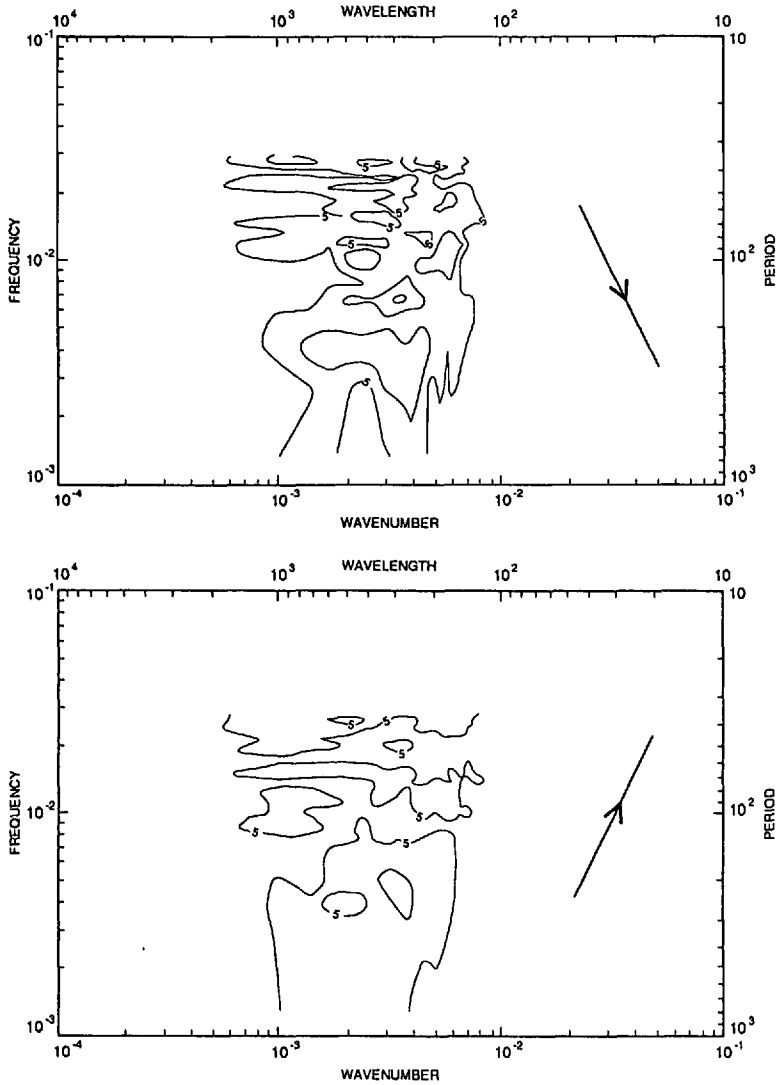

Figure 9. (Continued)

Comparing the spectra of the two areas in the eastern part of the basin with that of the Gulf Stream also explains the differences in time scale. In the east, there is little energy at periods of less than 100 days, while a signal is clearly observed for such periods in the Gulf Stream area. In addition, the lower frequency and particularly the seasonal signal is stronger, as a proportion of the total signal, in the east than the west. Thus, more than 55% of the total energy is found for periods longer than 250 days in the AC and NEA area while only 40% of the total energy is found at these periods in the GS area. As noted in Section 2, there is also apparently a relationship

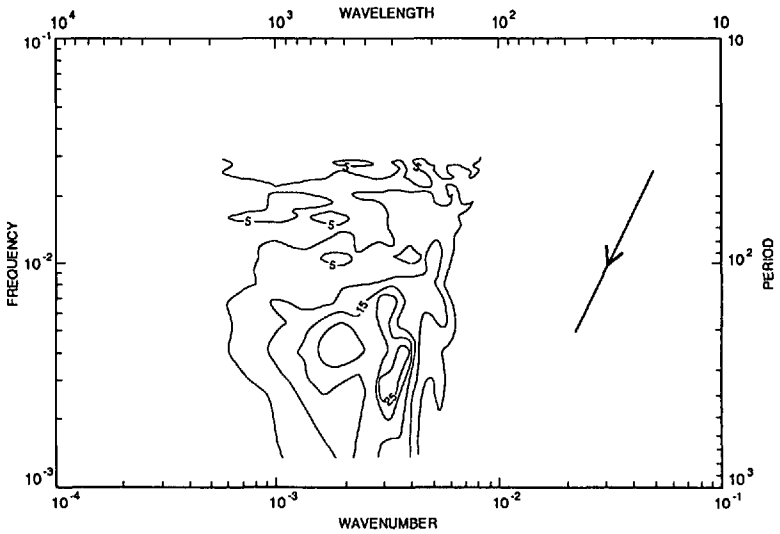

Figure 9. (Continued)

between strong temporal correlations and the bottom topography. The seasonal signal observed by Dickson *et al.* (1982) in the Northeast Atlantic has been interpreted in terms of topography as resulting from modulation of wind-forced topographic waves. However, this signal corresponds to a seasonal variation of high-frequency motions given the stronger wind fluctuations in winter and is not a one-year period signal. If the rather low frequencies observed by Geosat are related to bottom topography, this is probably due to trapping of eddies over topography. Treguier and Mc Williams (1990) have, indeed, investigated the topographic influence on a wind-driven stratified flow in a β-plane channel. They show that addition of bottom topography in their simulations produces a very significant increase of eddy time scales. These results suggest that bottom topography could explain the long time scales found above and east of the Mid-Atlantic-Ridge where the ocean floor is particularly rough. However, this would call for dedicated study beyond the scope of this study. Note also that wavenumber spectra (and space scales) seem also to be affected by the roughness of bottom topography in these areas (Le Traon *et al.*, 1990).

c. Pseudo-dispersion relations

To illustrate the relationship between space and time scales, pseudo-dispersion relations were calculated for the three study areas. A mean frequency $\langle\omega_1\rangle(k)$ is calculated for each wavenumber k by

$$\langle\omega_1\rangle(k) = \int E_1(k, \omega)\omega \, d\omega \,/\, \int E_1(k, \omega) \, d\omega \tag{5}$$

where $E_1(k, \omega)$ is the along-track frequency-wavenumber spectrum.

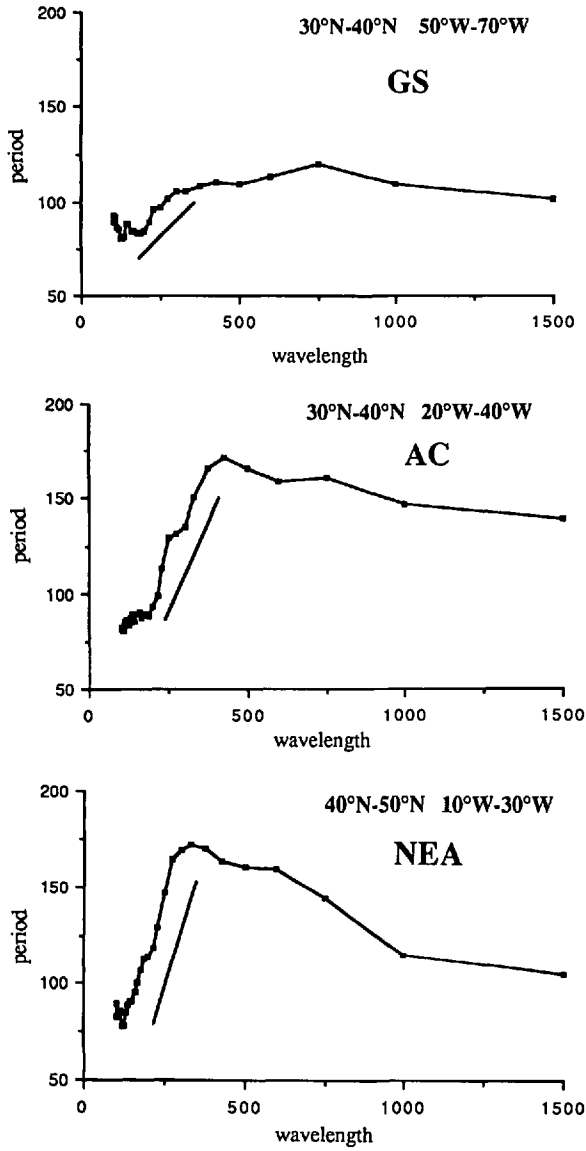

Figure 10. (a) Pseudo-dispersion relation for the Gulf Stream area. Straight line corresponds to a linear dispersion relation with $c = 6$ cms^{-1}. (b) Pseudo-dispersion relation for the Azores current area. Straight line corresponds to a linear dispersion relation with $c = 3$ cms^{-1}. (c) Pseudo-dispersion relation for the Northeast Atlantic area. Straight line corresponds to a linear dispersion relation with $c = 2$ cms^{-1}.

The dispersion relations giving mean periods T ($T = \langle\omega_1\rangle^{-1}$) as a function of wavelengths L ($L = k^{-1}$), are shown on Figures 10a, 10b and 10c. For short wavelengths, the relationship between wavelength and period is quasi-linear, of the form $L = cT$, where c is about 2–3 cms^{-1} for the AC and NEA areas and 5–6 cms^{-1} for

the GS areas. These propagation velocities agree with those deduced from Figure 6. This linear dispersion relation is characteristic of a turbulent regime where eddies advect one another past a fixed sensor in the advective time (Rhines, 1977). It is also observed in simulations of quasi-geostrophic turbulence (e.g. Hua and Haidvogel, 1986; Treguier and Hua, 1987). For the Gulf Stream area (see Fig. 10a), this linear relation is observed less clearly at short wavelengths. This is probably due to aliasing of the short time scales (less than 34 days).

It should be noted, however, that the pseudo-dispersion relations are calculated here from along-track spectra which contain contributions from all wavenumbers larger than k whose wavenumber vector components along the satellite ground track are k. However, if isotropy is assumed for each frequency ω (a quite restrictive assumption), the frequency-wavenumber scalar spectra $E_0(k, \omega)$ [$E_0(k, \omega) = 2\pi k \cdot E_2(k_1, k_2, \omega)$, where $E_2(k_1, k_2, \omega)$ is the two-dimensional (in space) frequency-wavenumber spectrum and where $k_1^2 + k_2^2 = k^2$] is related to $E_1(k, \omega)$ (e.g. Fu, 1983; Le Traon *et al.*, 1990) by

$$E_1(k, \omega) = \frac{2}{\pi} \int_k^\infty \frac{E_0(k_1, \omega)\, dk_1}{(k_1^2 - k^2)^{1/2}}. \tag{6}$$

The relationship between $\langle \omega_1 \rangle(k)$ and $\langle \omega_0 \rangle(k)$ [$\langle \omega_0 \rangle(k) = \int E_0(k, \omega)\, \omega\, d\omega / \int E_0(k, \omega)\, d\omega$] is obtained from (6):

$$\langle \omega_1 \rangle(k) E_1(k) = \frac{2}{\pi} \int_k^\infty \frac{E_0(k_1) \langle \omega_0 \rangle(k_1) dk_1}{(k_1^2 - k^2)^{1/2}} \tag{7}$$

where $E_1(k)$ and $E_0(k)$ are, respectively, the along-track and scalar wavenumber spectra.

Since a linear dispersion relation [i.e. $\langle \omega_1 \rangle(k) = c^{-1}k$, where c is a constant velocity] is observed for small wavelengths where along-track wavenumber spectra $E_1(k)$ are red with $E_1(k) = k^{-\alpha}$ and $2 < \alpha < 5$ (Le Traon *et al.*, 1990), it is straightforward from (7) that the dispersion relation $\langle \omega_0 \rangle(k)$ is also linear. So, this makes it likely that the real dispersion relation is linear at these wavelengths.

After this turbulent regime, the dispersion relations are different at the longest wavelengths, indicating a change in the dynamic regime. The change could correspond to a more linear dynamic regime. This is expected in quasi-geostrophic turbulence at the end of the nonlinear cascade when the dispersion of Rossby waves begins to dominate the oceanic signal (e.g. Rhines, 1977; Tréguier and Hua, 1989). Note, however, that the real dispersion cannot be calculated from (7) since the previous assumption of isotropy does not hold, of course, for Rossby waves. The interpretation is thus more difficult and can only be qualitative. For the AC and NEA areas, there is an inverse dispersion relation, i.e. long wavelengths associated with shorter time scales, while for the GS area, the mean periods remain approximately constant. In fact, for the Gulf Stream, the energy seen at the longest wavelengths

(>600 km) arises mainly from spatial aliasing of the shorter wavelengths which propagate in a non along-track direction (Le Traon *et al.,* 1990). On the other hand, for the other two areas and in particular the NEA area, there is a non-negligible signal at long wavelengths since the wavenumber spectra remain red at these wavelengths. Simulations of quasigeostrophic turbulence forced by fluctuating winds (Treguier and Hua, 1987) show clearly this change in dynamic regime, with a turbulent regime for the smaller scales and an essentially barotropic linear regime at longer wavelengths. This idea was put forward by Le Traon *et al.* (1990) in their analysis of the along-track wavenumber spectra. They suspected a change in dynamic regime after the wavenumber spectral peak. This seems to be confirmed here since the change in dispersion relation occurs at a wavelength comparable to the wavenumber spectral peak. Note, therefore, that this wavelength is larger for the AC area than for the NEA area, in agreement with wavenumber spectral peaks which are at about 400 km and 300 km for the AC and NEA areas respectively (Le Traon *et al.,* 1990). The inverse dispersion relation observed with Geosat data suggests that, at these scales, part of the oceanic variability is due to barotropic Rossby waves. However, the mean periods observed are too large to be due only to barotropic waves. Thus, barotropic Rossby waves of wavelength 500 km and 1000 km propagating in an along-track direction would have periods of respectively 90 and 45 days. These periods are shorter than those observed on Figures 10b and 10c and would be even shorter if the topography was considered (i.e. in the case of topographic Rossby waves). This would not be surprising since the oceanic signal at these scales could well be a combination of baroclinic and barotropic Rossby waves. Finally, note that the computed propagation velocities are westward at these scales in agreement with Rossby wave dynamics.

4. Summary and conclusions

A systematic study of time scales of mesoscale variability over the North Atlantic was done using two years of Geosat data. Time scales were first characterized in 10° latitude per 10° longitude bins as in Le Traon *et al.* (1990) who calculated space scales from the same data set. A more detailed description of time scales was then obtained by calculating a global map of temporal correlation after one cycle (17.05 days). Time scales compare well with existing in-situ measurements. They are shortest in areas of high mesoscale activity and/or strong mean currents (i.e. Gulf stream and North Atlantic Current), while relatively long time scales are found above the Mid-Atlantic Ridge and in the eastern part of the basin. Bottom topography appears to play an important role in the temporal coherence of mesoscale structures. In general, time scales are not proportional to space scales and propagation velocities obtained from the division of space scales by time scales appear to be minimal east of the Mid-Atlantic Ridge.

Frequency-wavenumber spectral analysis complemented this statistical descrip-

tion of mesoscale variability. It shows that the dominant wavelengths of around 200 to 500 km (depending on latitude) are associated with long periods (> 150 days) in the eastern part of the basin, while near the Gulf Stream significant energy is found at shorter periods. This explains in part why time scales are longer there. There is also apparently aliasing of short periods onto longer periods in the Gulf Stream area. In the Gulf Stream area, propagation velocities are either westward or eastward for short periods (< 80 days). At longer periods and in the North-East Atlantic, they are mainly westward. Quasi-seasonal signals associated with westward propagations are also observed in these frequency-wavenumber spectra.

Preliminary comparisons with quasigeostrophic turbulence models show qualitative agreement. They also confirm the interpretation of wavenumber spectra by Le Traon *et al.* (1990) who suspected a change in dynamic regime after the spectral peak in wavenumber. Indeed, pseudo-dispersion relations deduced from Geosat data point to two distinct dynamic regimes, as in models: a turbulent regime for smaller scales (< 300 to 500 km), where there is proportionality between space and time scales, and an apparently more linear regime after the spectral peak in wavenumber where an inverse dispersion relation is found in the eastern part of the basin. This latter feature is in agreement with quasigeostrophic models forced by fluctuating winds.

Acknowledgments. We thank P. Gaspar and J. F. Minster for helpful discussions. Geosat data were processed at GRGS/UMR39 (Groupe de Recherche en Géodésie Spatiale). This study was supported by SHOM/GERDSM/CLS ARGOS contract no. A 89 48 648 00.

REFERENCES

Bisagni, J. J. 1989. Wet tropospheric range corrections for satellite altimeter-derived dynamic topographies in the Western North Atlantic. J. Geophys. Res., *94,* 3247–3254.

Bretherton, F. P., R. E. Davis and C. B. Fandry. 1976. A technique for objective analysis design of oceanographic experiments applied to Mode 73. Deep-Sea Res., *23,* 559–582.

Cheney, R. E., B. C. Douglas, R. W. Agreen, L. Miller, D. Milbert and D. L. Porter. 1986. The Geosat altimeter mission: a milestone in satellite oceanography. EOS Trans. AGU, *67*(48), 1354–1355.

Cheney, R. E., B. C. Douglas, R. W. Agreen, L. Miller, D. L. Porter and N. S. Doyle. 1987. Geosat altimeter geophysical data record user handbook. National Ocean Service/NOAA, Rockville, MD.

Colin de Verdière, A., H. Mercier and M. Arhan. 1989. Mesoscale variability transition from the western to the eastern Atlantic along 48N. J. Phys. Oceanogr., *19,* 1149–1166.

De Mey, P. and Y. Menard. 1989. Synoptic analysis and dynamical adjustment of Geos3 and Seasat altimeter eddy fields in the North West Atlantic. J. Geophys. Res., *94,* 6221–6230.

Dickson, R. R. 1983. Global summaries and intercomparisons: Flow statistics from long-term current meter mooring, *in* Eddies in marine science, A. R. Robinson ed., Springer-Verlag, Berlin, 609 pp.

Dickson, R. R., W. J. Gould, P. A. Gurbutt and P. D. Killworth. 1982. A seasonal signal in ocean currents to abyssal depths. Nature, *295,* 193–198.

Fu, L. L. 1983. On the wave number spectrum of oceanic mesoscale variability observed by the SEASAT altimeter. J. Geophys. Res., *88,* 4331–4341.

Fu, L. L., J. Vasquez and M. E. Parke. 1987. Seasonal variability of the Gulf Stream from satellite altimetry. J. Geophys. Res., *92,* 749–754.

Fu, L. L. and V. Zlotnicki. 1989. Observing oceanic mesoscale eddies from Geosat altimetry: preliminary results. Geophys. Res. Lett., *16,* 457–460.

Gould, W. J. 1983. The Northeast Atlantic Ocean, *in* Eddies in Marine Science. A. R. Robinson ed., Springer-Verlag, Berlin, 609 pp.

1985. Physical oceanography of the Azores front. Prog. in Oceanogr., *14,* 167–190.

Hamming, R. W. 1977. Digital filters, Prentice Hall signal processing series, A. V. Oppenheim series editor.

Hayashi, Y. 1973. A method of analysing transient waves by space-time cross spectra. J. Appl. Meteo., *12,* 404–408.

Hua, B. L. and D. B. Haidvogel. 1986. Numerical simulations of the vertical structure of quasi-geostrophic turbulence. J. Atmos. Sci., *43,* 2923–2936.

Jourdan, D. 1990. Observation des structures océaniques par altimétrie satellitaire: influence des corrections d'environnement sur la restitution du signal mésoéchelle, Thèse de doctorat de l'Université Paul Sabatier, 171 pp.

Käse, R. H., W. Zenk, T. B. Sanford and W. Hiller. 1985. Currents, fronts and eddy fluxes in the Canary basin. Progr. in Oceanogr., *14,* 231–257.

Klein, B. and G. Siedler. 1989. On the origin of the Azores current. J. Geophys. Res., *94,* 6159–6168.

Le Groupe Tourbillon. 1983. The Tourbillon experiment: a study of a mesoscale eddy in the eastern North Atlantic. Deep-Sea Res., *30,* 475–511.

Le Traon, P. Y., C. Boissier and P. Gaspar. 1991. Analysis of errors due to polynomial adjustments of altimeter profiles. J. Atm. Ocean. Tech., *8,* 385–396.

Le Traon, P. Y., M. C. Rouquet and C. Boissier. 1990. Spatial scales of mesoscale variability in the North Atlantic as deduced from Geosat data. J. Geophys. Res., *95,* 20,267–20,285.

Lippert A. and M. Briscoe. 1990. Observations and EOF analysis of low frequency variability in the western part of the Gulf Stream circulation. J. Phys. Oceanogr., *20,* 646–656.

Mercier, H. and A. Colin de Verdière. 1985. Space and time scales of mesoscale motions in the Eastern North Atlantic. J. Phys. Oceanogr., *15,* 171–183.

Monaldo, F. 1990. Path length variations caused by atmospheric water vapor and their effects on the measurement of mesoscale ocean circulation features by a radar altimeter. J. Geophys. Res., *95,* 2923–2932.

Monin, A. S. and A. M. Yaglom. 1971. Statistical Fluid Mechanics, vol. 1, MIT Press.

Parke, Y. H., 1990. Mise en évidence d'ondes planétaires semi-annuelles dans le sud de l'océan indien par altimétrie satellitaire. C.R. Acad. Sci. Paris, *310,* 2,919–926.

Rhines, P. B., 1977. The dynamics of unsteady currents, *in* The Sea, *6,* Marine modelling, E. D. Goldberg, I. N. McCave, J. J. O'Brien and J. H. Steele, eds., 189–318, John Wiley, NY.

Richardson, P. L. 1983. Gulf Stream rings, *in* Eddies in Marine Science, A. R. Robinson ed., Springer-Verlag, Berlin, 609 pp.

Richman, J. G., C. Wunsch and N. G. Hogg. 1977. Space and time scales of mesoscale motion in the Western North Atlantic. Rev. of Geophys. and Space Phys., *15,* 385–420.

Saunders, P. M. 1982. Circulation in the Eastern North Atlantic. J. Mar. Res., *40*(Supp.), 641–657.

Siedler, G., W. Zenk and W. J. Emery. 1985. Strong current events related to a subtropical front in the Northeast Atlantic. J. Phys. Oceanogr., *15,* 885–897.

Stommel, H. 1965. The Gulf Stream: A Physical and Dynamical Description. 2nd ed., University of California Press, Berkeley, 248 pp.

Stramma, L. and G. Siedler. 1988. Seasonal changes in the North Atlantic subtropical gyre. J. Geophys. Res., *93,* 8111–8118.

Treguier, A. M. and B. L. Hua. 1987. Oceanic quasi-geostrophic turbulence forced by stochastic wind fluctuations. J. Phys. Oceanogr., *17,* 397–411.

Treguier, A. M. and J. C. McWilliams. 1990. Topographic influences on wind-driven, stratified flow in a β-plane channel: an idealized model for the Antarctic circumpolar current. J. Phys. Oceanogr., *20,* 321–343.

White, W. B., C. K. Tai and W. R. Holland. 1990. Continuous assimilation of Geosat altimetric sea level observations into a numerical synoptic ocean model of the California current. J. Geophys. Res., *95,* 3127–3148.

Willebrand, J. 1978. Temporal and spatial scales of the wind field over the North Pacific and North Atlantic. J. Phys. Oceanogr., *8,* 1080–1094.

Wunsch, C. 1983. Western North Atlantic interior, *in* Eddies in Marine Science, A. R. Robinson ed., Springer-Verlag, Berlin, 609 pp.

Zlotnicki, V., L. L. Fu and W. Patzert. 1989. Seasonal variability in global sea level observed with Geosat altimetry. J. Geophys. Res., *94,* 17959–17969.

Received: *15 January, 1991;* revised: *11 June, 1991.*